Hydrogen-Induced Structural Changes at the Nickel Site of the Regulatory [NiFe] Hydrogenase from *Ralstonia eutropha* Detected by X-ray Absorption Spectroscopy†

Michael Haumann,*,‡ Antje Porthun,§ Thorsten Buhrke,§ Peter Liebisch,‡ Wolfram Meyer-Klaucke,|| Bärbel Friedrich,§ and Holger Dau‡

Institut für Experimentalphysik, Freie Universität Berlin, Arnimallee 14, D-14195 Berlin, Germany, Mikrobiologie, Humboldt-Universität zu Berlin, Chausseestrasse 117, D-10115 Berlin, Germany, and EMBL Outstation, DESY, Notkestrasse 85, D-22603 Hamburg, Germany

Received May 15, 2003; Revised Manuscript Received July 14, 2003

ABSTRACT: For the first time, the nickel site of the hydrogen sensor of *Ralstonia eutropha*, the regulatory [NiFe] hydrogenase (RH), was investigated by X-ray absorption spectroscopy (XAS) at the nickel K-edge. The oxidation state and the atomic structure of the Ni site were investigated in the RH in the absence (air-oxidized, RH^{ox}) and presence of hydrogen (RH^{+H2}). Incubation with hydrogen is found to cause remarkable changes in the spectroscopic properties. The Ni-C EPR signal, indicative of Ni(III), is detectable only in the RH^{+H2} state. XANES and EXAFS spectra indicate a coordination of the Ni in the RH^{ox} and RH^{+H2} that pronouncedly differs from the one in standard [NiFe] hydrogenases. Also, the changes induced by exposure to H_2 are unique. A drastic modification in the XANES spectra and an upshift of the K-edge energy from 8339.8 (RH^{ox}) to 8341.1 eV (RH^{+H2}) is observed. The EXAFS spectra indicate a change in the Ni coordination in the RH upon exposure to H_2. One likely interpretation of the data is the detachment of one sulfur ligand in RH^{+H2} and the binding of additional (O,N) or H ligands. The following Ni oxidation states and coordinations are proposed: five-coordinated $Ni^{II}(O,N)_2S_3$ for RH^{ox} and six-coordinated $Ni^{(III)}$-$(O,N)_3X_1S_2$ [X being either an (O,N) or H ligand] for RH^{+H2}. Implications of the structural features of the Ni site of the RH in relation to its function, hydrogen sensing, are discussed.

[NiFe] hydrogenases are widespread among prokaryotes and lower eukaryotes. They catalyze the reversible heterolytic cleavage of molecular hydrogen into two protons and two electrons. [NiFe] hydrogenases are redox proteins possessing an active site which contains one Ni and one Fe atom (for reviews, see refs *1*−*5*). Hydrogenases represent phylogenetically ancient systems, developed for energy production in extreme and often anaerobic environments (*6*). As a consequence, most hydrogenases are inactivated by molecular oxygen.

The facultative chemolithoautotrophic bacterium *Ralstonia eutropha* (formerly designated *Alcaligenes eutrophus*) has acquired the ability to use hydrogen as an energy source under aerobic conditions. Genetic exploration of the synthesis and regulation of the three [NiFe] hydrogenases resident in this organism has revealed a complex multicomponent system, designed to efficiently detect and process the small hydrogen molecule (*7*, *8*).

(1) The membrane-bound hydrogenase (MBH) is linked to the respiratory chain. (*2*) The main function of the cytoplasmic soluble NAD-linked hydrogenase (SH)[1] is to provide reducing equivalents for CO_2 fixation (*9*). (*3*) A particularly interesting new type of hydrogenases has only recently been discovered in *R. eutropha*, the so-called regulatory hydrogenase (RH) (*10*). The RH belongs to the subclass of H_2-sensing [NiFe] hydrogenases (*11*). H_2 sensors of the RH type have also been found in *Rhodobacter capsulatus* (*60*) and *Bradyrhizobium japonicum* (*61*).

The RH of *R. eutropha* is the subject of this study. It senses the presence of small amounts of hydrogen in the medium, thereby initiating a complex signal transduction cascade which finally leads to the expression of the energy-converting hydrogenases (*8*, *11*). Unlike the oxygen-sensitive "standard" hydrogenases from most other organisms, the physiologically distinct [NiFe] hydrogenases of *R. eutropha* are fully active in the presence of molecular oxygen (*8*).

Recent studies of the RH have revealed unusual biochemical features (*12*). This hydrogenase is always "on alert", ready to react with hydrogen, as concluded from the absence of a lag phase at the onset of hydrogen cleavage (*13*). A reductive activation of the RH is not necessary. Its rate of

† We gratefully acknowledge funding by the Deutsche Forschungsgemeinschaft within SFB 498 (for M.H., P.L., and H.D. within projects C8 and C6 and for A.P., T.B., and B.F. within project C1). A.P., T.B., and B.F. also thank the Fonds der Chemischen Industrie for financial support. W.M.-K. is the EMBL station scientist at beamline D2 of HASYLab/DESY Hamburg.

* To whom correspondence should be addressed: Physik, Freie Universität Berlin, Arnimallee 14, D-14195 Berlin, Germany. Telephone: ++49 30 8385 6101. Fax: ++49 30 8385 6299. E-mail: haumann@physik.fu-berlin.de.

‡ Freie Universität Berlin.

§ Humboldt-Universität zu Berlin.

|| DESY.

[1] Abbreviations: DFT, density functional theory; DTT, dithiothreitol; ENDOR, electron nuclear double-resonance spectroscopy; EPR, electron paramagnetic resonance spectroscopy; EXAFS, extended X-ray absorption fine structure; FTIR, Fourier transform infrared spectroscopy; RH, regulatory [NiFe] hydrogenase; RH^{+H2}, H_2-flushed RH; RH^{ox}, air-oxidized RH; SH, NAD-linked hydrogenase; XANES, X-ray absorption near-edge structure; XAS, X-ray absorption spectroscopy.

10.1021/bi034804d CCC: $25.00
Published on Web 08/26/2003

hydrogen cleavage, however, is at least 100 times lower than that of standard [NiFe] hydrogenases (*15*). From FTIR and EPR experiments, it has been concluded that, unlike other [NiFe] hydrogenases which exhibit up to seven redox states (for a review, see ref *4*), the RH exists in only two redox states, namely, in the air-oxidized form and in a second form which develops upon exposure to H_2. The latter exhibits an EPR signal (*13*, *15*) due to a paramagnetic state of the Ni, termed Ni-C, which has also been observed in other hydrogenases and is now commonly attributed to a Ni(III) oxidation state (*13*, *16*). The binding of two CN^- ligands and one CO group to the Fe in the RH active site has been revealed by FTIR experiments (*15*). In this respect, the RH resembles the standard type of [NiFe] hydrogenase (*2*, *17*, *18*). Interestingly, unlike in standard cases, no indications for redox reactions of Fe−S clusters have been obtained for the RH. On the other hand, in the presence of H_2, the EPR-invisible reduction of a nonmetal cofactor, possibly a two-electron-accepting nucleotide derivative, has been detected by optical spectroscopy (*15*). As the RH forms a double dimer (*7*, *10*), the nonmetal cofactor may accept one electron from each RH unit (*15*).

It is commonly believed that the properties of the Ni site are critical for hydrogen cleavage by all [NiFe] hydrogenases (*3*, *4*, *20*). The crystal structures of several [NiFe] hydrogenases from anaerobic organisms have been resolved (*2*, *20*, and references therein). They revealed the binding of the Ni atom by four thiol groups of cysteine residues of the protein and a Ni−Fe distance of ∼2.5−3 Å, depending on the redox state. So far, crystals of hydrogenases from aerobic sources have not been obtained. Thus, at present, the reasons for the "unusual" catalytic behavior of the RH are unclear, and information about the coordination of the Ni atom in the active site is required to provide clues about the mechanism of hydrogen sensing.

In this work, we contribute the first X-ray absorption spectroscopy (XAS) results on the structure of the Ni site in the RH. XAS can resolve the neighboring atoms of the Ni (*27*, *57*, *74*), thereby, in principle, allowing for the construction of an atomic model of the Ni site at subangstrom resolution. We find pronounced changes in the Ni coordination in the RH upon its exposure to H_2. Possible relations between the structural features of the Ni site of the RH and its special catalytic properties are discussed.

MATERIALS AND METHODS

Purification of the Regulatory Hydrogenase (RH) and Sample Preparation. The RH was isolated from *R. eutropha* HF371(pGE378), a derivative of *R. eutropha* H16 that allows RH overexpression (*11*). The strain was cultivated in mineral medium under hydrogenase derepressing conditions at 30 °C. Cells were harvested by centrifugation, washed once in 50 mM potassium phosphate buffer (pH 7), and stored frozen in liquid nitrogen. For RH purification, 90 g of cells (wet weight) was resuspended in 35 mL of 50 mM KPO_4 buffer (pH 7) containing 0.1 mM phenylmethanesulfonyl fluoride. Cells were disrupted in a French pressure cell at 1100 lb per square inch. The soluble extract was prepared by high-speed centrifugation (100000*g* for 60 min at 4 °C). RH purification included a heat treatment step, hydrophobic interaction, and anionic exchange chromatography as described previously (*15*). Finally, the purified sample was dialyzed against 20 mM Tris-HCl buffer (pH 8), concentrated with Centriprep-10 and Microcon (Amicon) instruments according to the manufacturers' instructions to ∼50 mg/mL protein (0.57 mM RH), and directly frozen in liquid nitrogen. Protein concentrations were determined by the method of Bradford (*21*). H_2-oxidizing activity was quantified by an amperometric H_2 uptake assay as described previously (*13*). Seven different preparations of the RH with specific activities of 0.5 ± 0.1 unit/mg were used in this work. RH samples were used as aerobically isolated (RH^{ox}), or the purified enzyme was incubated with 100% hydrogen for 3−25 min (RH^{+H2}). Hydrogenase samples were added to sample holders with Kapton windows for XAS and EPR measurements (ca. 40 μL of protein solution per sample holder) under an argon atmosphere and rapidly frozen in liquid nitrogen.

X-ray Absorption Spectroscopy. X-ray absorption spectra at the nickel K-edge were collected at beamline D2 of the EMBL Hamburg outstation (HASYLAB, DESY). Fluorescence-detected X-ray absorption spectra were measured at 20 K as described elsewhere (*22*; monochromator detuning to 70% of the maximum intensity, scan range of 8150−9100 eV). An absolute energy calibration was performed by monitoring the Bragg reflections of a crystal positioned at the end of the beamline (*23*). For each element of the 13-element solid state germanium detector that was used, the total count rate was kept below 30 000; the output signal was corrected for detector saturation. The spot size of the X-ray beam on the sample was 4.75 mm × 1 mm; not more than three scans with a duration of ∼60 min were taken on the same spot of the sample. Comparison of the first and third scan revealed no evidence of radiation damage to the samples (the Ni K-edge energy remained constant within ±0.1 eV). Eight to twelve scans, obtained on four separate spots of the samples, were averaged for each EXAFS spectrum.

Spectra were normalized and EXAFS oscillations extracted as described in ref *22*. The energy scale of Ni EXAFS spectra was converted to a k scale using an E_0 of 8333 eV (*24*); E_0 was refined to 8335 eV during the simulation of EXAFS spectra. Unfiltered k^3-weighted spectra were used for least-squares curve fitting [with the in-house software SimX (*25*)] and for calculation of Fourier transforms. The shown Fourier transforms represent k values ranging from 1.85 to 12.8 $Å^{-1}$. The data were multiplied by a fractional cosine window (10% cosine fraction at low and high k side). For EXAFS simulation, complex back-scattering amplitudes were calculated using FEFF 7 (*51*); the value of S_0^2, the amplitude reduction factor, was 0.9. This value facilitated the correct determination of the coordination number of six from the EXAFS spectrum of the $Ni(H_2O)_6$ complex. The given "K-edge energies" refer to 50% of the normalized absorption at the Ni K-edge.

EPR Spectroscopy. EPR spectroscopy was performed using a Bruker ESP 300E spectrometer equipped with a helium cryostat (laboratory of W. Lubitz and F. Lendzian, Technical University Berlin, Berlin, Germany). EPR measurements were carried out at a temperature of 6.5 K; the other conditions were as follows: microwave frequency of 9.59 GHz, microwave power of 250 μW, modulation frequency of 10 kHz, and modulation amplitude of 2 mT. EPR spectra were normalized with respect to the same enzyme content of samples.

Table 1: Ni K-Edge (XANES) Features of the RH in the Absence and Presence of Hydrogen[a]

RH state	Ni oxidation state	K-edge energy (eV, ±0.1)	maximal intensity (±0.03)	pre-edge peak area ($\times 10^{-2}$ eV, ±0.5)	K-edge shape
RH^{ox}, as-isolated, fully air-oxidized	Ni(II)	8339.8	1.07	3.9	rounded, shoulder at ~8337 eV
RH^{+H2}, flushed with H_2 for 10 min	Ni(III)	8341.1	1.35	2.4	sharp
RH, as-isolated, incompletely air-oxidized	Ni(II)/Ni(III)	8340.6	1.14	3.1	intermediate
RH, as-isolated, incompletely air-oxidized, with DTT	Ni(II)	8339.5	1.05	4.1	rounded, shoulder at ~8337 eV
RH, flushed with H_2 for 3 min	Ni(II)/Ni(III)	8341.0	1.25	2.6	intermediate
$Ni(H_2O)_6$	Ni(II)	8341.9	1.82	2.2	sharp

[a] K-edge energies correspond to 50% of the normalized fluorescence intensities (see Figure 1). The pre-edge peak areas were determined from the integration of pre-edge peaks as shown in Figure 1 (see the legend). The Ni(III) oxidation state is characterized by the Ni-C EPR signal. The maximal intensity refers to the normalized fluorescence at 8350 eV on top of the K-edge. The $Ni(H_2O)_6$ data have been derived from a 5 mM aqueous solution of $NiCl_2$.

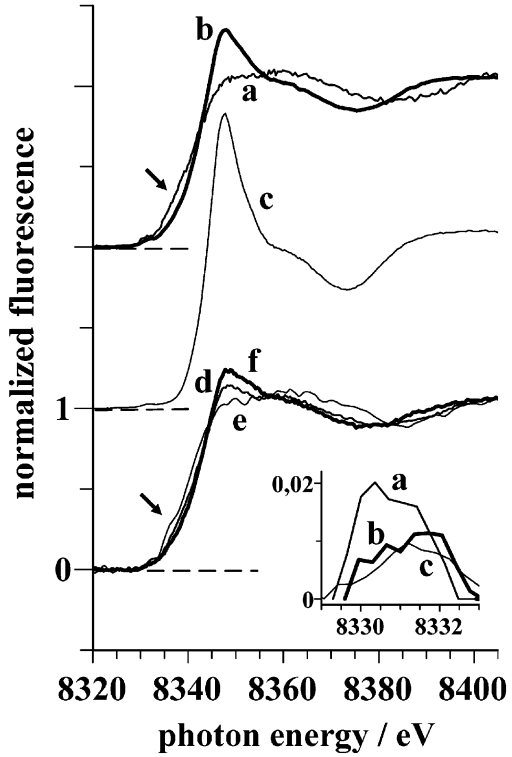

FIGURE 1: XANES spectra of the RH as a function of redox poise: (a) RH^{ox} (as-isolated, fully air-oxidized, thin line), (b) RH^{+H2} (H_2 flushing for 10 min, thick line), (c) $Ni(H_2O)_6$ from a 5 mM aqueous $NiCl_2$ solution, (d) RH (as-isolated, incompletely air-oxidized, medium line), (e) RH (incompletely air-oxidized with 0.5 mM DTT, thin line), and (f) RH (H_2 flushing for 3 min). The inset shows the isolated pre-edge peaks as obtained after the subtraction of a polynomial from the XANES spectra for removal of the edge background: (a) RH^{ox}, (b) RH^{+H2}, and (c) $Ni(H_2O)_6$. Spectra have been equally scaled and in part vertically displaced for better comparison. The arrows mark the shoulder in the rising part of the edge.

RESULTS

XANES Spectra

XANES spectra at the Ni K-edge (Figure 1) were recorded with the RH in the air-oxidized form (RH^{ox}, trace a) and after flushing of the enzyme with hydrogen for 10 min (RH^{+H2}, trace b). Visual inspection of the spectra immediately reveals that exposure to H_2 causes a drastic change in the shape of the Ni K-edge. In the RH^{ox} (Figure 1), the edge is relatively broad and exhibits an unresolved shoulder at ~8337 eV. The edge energy (energy corresponding to 50% of the normalized intensity) equals 8339.8 eV (Table 1). In the RH^{+H2}, the edge becomes much sharper, showing a pronounced peak at ~8350 eV which is almost absent in the RH^{ox}. The edge position, 8341.1 eV, is clearly shifted by 1.3 eV to higher energies in the RH^{+H2}. A shift to higher energies from ~8330.5 to ~8331.5 eV is also apparent in the position of the maximum of the pre-edge peak feature (inset in Figure 1).

Increasing the hydrogen incubation time from 10 to 25 min did not increase the differences in the XANES spectra (not documented). Shorter H_2 incubation (3 min) resulted in a spectrum (Figure 1, trace f) that was between (Table 1) the RH^{ox} (trace a) and RH^{+H2} (exposure to H_2 for 10 min, trace b) spectra. Thus, it is likely that the latter sample has been essentially completely (>90%) in the RH^{+H2} state. In some preparations of the RH, the "as-isolated" state revealed a XANES spectrum with a K-edge shape somewhat sharper and a maximal intensity higher (Figure 1, trace d) than those observed in the RH^{ox} sample (Figure 1, trace a). According to the observation of a small Ni-C EPR signal (not shown; see below) in this sample, it contains a small portion of the RH^{+H2} state. Since the purification protocol for the RH includes a heat treatment step that is carried out in the presence of hydrogen (*15*), the population of reduced RH proteins that sometimes appear in as-isolated samples can be explained by incomplete reoxidation of the protein which is due to the high stability of the H_2-induced state (*15*). Incubation of this sample with a chemical reductant (DTT, $E_0^{pH\ 7} = -330$ mV) produced a XANES spectrum (Figure 1, trace e) similar to the one observed for the RH^{ox} sample (trace a). Apparently, DTT reduces all residual Ni(III) to the Ni(II) oxidation state. Consequently, we conclude that >90% of Ni was present as Ni(II) in the RH^{ox} sample. The above experiment furthermore rules out any significant contamination of the samples with free Ni [the XANES spectrum of aqueous $Ni^{(II)}(H_2O)_6$ (Figure 1, trace c) is insensitive to DTT].

In general, the K-edge shape and energy of protein-bound metals are expected to be sensitive to the ligand environment of the metal and to its oxidation state (*26*, *27*, *74*). Consequently, information about the first coordination sphere of Ni can be obtained by analysis of XANES spectra.

K-Edge Energy. An energy value describing the position of the K-edge has diagnostic value in the determination of the oxidation state; frequently, an increase in this edge energy upon oxidation of the metal is observed (for a review, see ref *74*). However, a less straightforward relation has been observed in Ni model compounds (*28*, *29*) and in [NiFe]

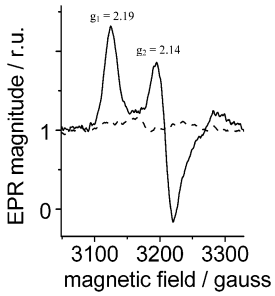

FIGURE 2: EPR spectra of the RH in the presence and absence of H_2. EPR spectra have been obtained from the same samples that have been used for XAS: RH^{ox} (as-isolated, fully air-oxidized, dotted line) and RH^{+H2} (H_2 flushing for 10 min, solid line). Only the low-field parts of the spectra are shown because in the region around $g = 2$ a sharp signal from the acrylic−glass sample holders was overlapping. The indicated g values are similar to the previously observed ones (*15*).

hydrogenases, in the presence of mixed [(O,N),S] ligation of the Ni. The largest edge shifts to higher energies upon oxidation of Ni(II) to Ni(III) (up to ∼1.5 eV) are observed in Ni models with only (O,N) ligands. In Ni oxy compounds, the Ni K-edge position has been found to be linearly related to the Ni oxidation state, yielding values of ∼8338.0 eV for Ni(I), ∼8338.7 eV for Ni(II), ∼8341.0 eV for Ni(III), and ∼8342.8 eV for Ni(IV) compounds (*30*). Intermediate K-edge shifts are obtained for mixtures of (O,N) and S ligands (0.4−0.6 eV), and negligible shifts are observed when only S ligands are present (*29*). The observation of overall smaller edge shifts in the presence of sulfur ligands can be explained by the more covalent character (compared to that of O or N ligands) of their binding to Ni. The latter situation may cause significant unpaired spin density on the sulfur ligands and thereby a higher degree of "delocalization" of the Ni charge (*29*, *72*). In line with this view, a ligand exchange from N_2S_4 to N_4S_2 in Ni(II) compounds already may yield an edge shift of ∼0.5 eV (*29*).

Taking these results together, the large edge shift upon formation of the RH^{+H2} state (1.3 eV) points toward (i) the presence of a mixed (O,N),S coordination of the Ni in the RH, (ii) an increase in the (O,N) to S ratio in the RH^{+H2}, and (iii) a change of the oxidation state from Ni(II) to Ni(III) in the RH^{+H2}.

To verify the Ni oxidation state, we carried out EPR measurements on the same samples that have subsequently been used for XAS investigations. In the RH^{ox} sample, no EPR signal was detected [Figure 2 (···)]. In the RH^{+H2}, on the other hand, a typical Ni-C EPR signal was observed [Figure 2 (—)]. This result is consistent with previous observations (*13*, *15*). The Ni-C EPR signal has been proposed to be due to a $^1/_2$ spin state arising from Ni(III) or Ni(I) species (*31*, *32*). A pure Ni(I) oxidation state is unlikely in the RH^{+H2} because the K-edge energy in Ni(I) compounds is obviously too low (∼8335−8338 eV) (*30*, *33*). Thus, the XANES data of the RH^{+H2} strengthen the notion that in the Ni-C state a formal Ni(III) oxidation state is present.

Magnitude of the K-Edge. The "sharpness" and height of the maximum of the Ni K-edge have been empirically related to the ligand environment of the Ni in model compounds; a sharper edge with a greater maximum, as in the RH^{+H2} (Figure 1), is indicative of a Ni environment dominated by "hard" (O,N) ligands, whereas a more rounded edge, as in the RH^{ox}, is indicative of larger numbers of "soft" sulfur ligands (*28*, *29*, *52*).

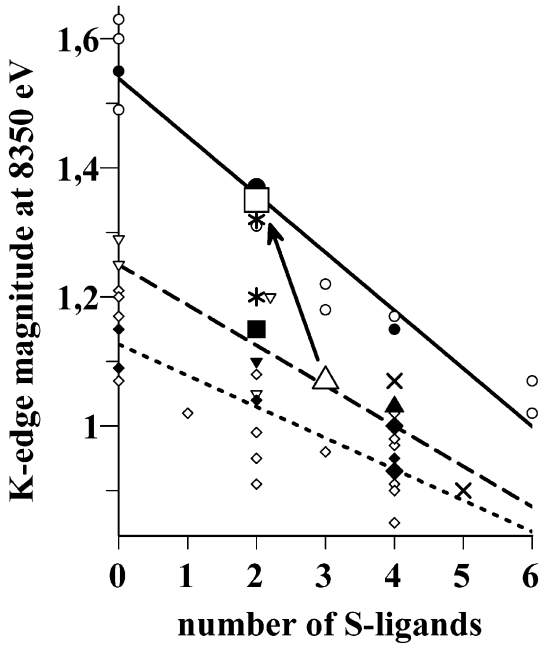

FIGURE 3: K-edge intensity vs the number of S ligands to the Ni. Data from Ni(II) model compounds (small empty symbols) have been taken from refs *28*, *29*, *32*, *33*, *52*, *53*, and *73*. Data from Ni(III) compounds (small filled symbols) have been taken from refs *29*, *30*, and *33*. Only models with pure N/S or O/S Ni coordinations have been considered. Straight lines represent linear fits to the experimental data for six-coordinated (○ and ●, solid line), five-coordinated (▽ and ▼, dashed line), and four-coordinated (◇ and ◆, dotted line) Ni(II)/(III) compounds. The large symbols denote data from [NiFe] hydrogenases: (△) RH^{ox}, (□) RH^{+H2}, (▲) oxidized *D. gigas* (*24*, *25*), (■) oxidized and Ni-C of *T. roseopersicina* (*63*), (◆) Ni-S_{i-r} (lower point) and Ni-C (upper point) of *C. vinosum* (*37*), and (●) oxidized SH of *R. eutropha* (average of data from refs *24* and *34*). Data for specific model compounds are shown as ∗ for N_3S_2 (lower point) and $N_3(O,N)_1S_2$ (upper point) (*32*) and × for P_4S_1 (lower point) and P_4H_1 (upper point) (*29*) (in the latter case, the P ligands are here considered to be equivalent to S ligands). For further details, see the text.

In Figure 3, relevant information from the literature (see the legend of Figure 3) about the intensity of the Ni K-edge in relation to the coordination number and to the (O,N)/S ratio of ligands is compiled. In Ni(II) model compounds, the maximum (at 8350 eV) decreases approximately linearly with an increasing number of S ligands (small empty symbols and straight lines in Figure 3). At a given number of S ligands, the highest maxima are observed in six-coordinated compounds, intermediate ones in five-coordinated compounds, and the smallest values in four-coordinated compounds. [We note that the straight lines in Figure 3 are not intended to mean that the correlation between the edge maximum and the number of S ligands is strictly linear. However, at present, there seems to be no indication of a systematic deviation from linearity. Thus, the lines represent a reasonable approximation of the data. We have also included data points for Ni(III) compounds in Figure 3 (small filled symbols). These points fall very close to the lines drawn through the data denoting Ni(II) compounds, as expected on basis of the observation that the edge maximum and shape in isoleptic models are only marginally affected by the Ni oxidation state (*29*).] The magnitude of the K-edge of the oxidized standard [NiFe] hydrogenase from *De-*

sulfovibrio gigas (*24*, *55*) [Figure 3 (▲)] where the Ni is known to be O_1S_4-coordinated (*17*) fits well to the data from five-coordinated model compounds [Figure 3 (dashed line)]. The magnitude of the K-edge of the RH^{ox} is represented by empty triangles (△) in Figure 3. The comparison with the literature results suggests for the RH^{ox} (i) a five-coordinated Ni and (ii) the presence of three S ligands.

In the RH^{+H2}, a pronounced increase in the K-edge maximum is observed. Such an increase is not observed in standard hydrogenases upon formation of the Ni-C state (see refs *24* and *37* and Figure 3). A XANES spectrum with a maximum higher than the one observed in other standard hydrogenases has only been obtained in the hydrogenase of *Thiocapsa roseopersicina* (*24*, *41*). In the latter enzyme, the Ni has been proposed to be five-coordinated to six-coordinated and, independent of the oxidation state, by only two S ligands from EXAFS analysis (*41*, *63*). The XANES spectrum of *T. roseopersicina* is compatible with this notion [Figure 3 (■)]. In the RH^{+H2}, the maximum is larger than in any of the investigated standard hydrogenases. Upon oxidation from Ni(II) to Ni(III) in isoleptic Ni model compounds, without a change in the number and chemical identity of ligands, the overall edge shape and magnitude remain about the same (*29*). We conclude that (i) the strong change in the Ni K-edge in the RH^{+H2} cannot simply be explained by a redox change in the Ni. It is rather indicative of a change in the Ni coordination. (ii) The magnitude of the K-edge of the RH^{+H2} in Figure 3 (□) implies a six-coordinated Ni and (iii) is most compatible with only two S ligands.

Pre-Edge Peak Area and p_z Shoulder. The intensity (area) of the pre-edge peak of the K-edge at ∼8331 eV is attributed to the dipole-forbidden electronic transition of the 1s core electron to bound unoccupied d levels. If a distortion from the octahedral coordination geometry occurs, the 1s → 3d transition gains intensity due to enhanced p−d mixing (*26*, *27*). The pre-edge peak area (Figure 1, inset, trace a; Table 1) is larger than in more symmetrical four- and six-coordinated Ni compounds (*29*), suggesting a five-coordinated Ni in the RH^{ox}. Further evidence for a five-coordinated Ni comes from the observation of a shoulder at ∼8337 eV in the rising part of the edge [Figure 1, trace a and also trace e (see below), arrows]. This shoulder has been ascribed to a low-energy 1s → $4p_z$ transition (with shakedown contributions) which is observed if a distortion from the ideal octahedral coordination geometry occurs (*29*, *52*, *56*, *74*). An octahedral geometry is present, e.g., in the Ni hexaquo complex $[Ni(H_2O)_6]$ where such a shoulder is absent (Figure 1, trace c). Thus, in the RH^{ox}, the geometry of ligands deviates from an octahedral coordination as is expected for a five-coordinated Ni.

In the RH^{+H2}, the pre-edge peak area (Figure 1, inset, trace b; Table 1) was approximately halved. In isoleptic model compounds, on the other hand, it has been shown that upon oxidation of Ni(II) to Ni(III) the pre-edge peak area is approximately doubled (*29*). The decrease in the pre-edge peak area thus most likely cannot be explained by a redox change in the Ni but rather by the presence of a six-coordinated Ni in the RH^{+H2}. Both the similar pre-edge peak area in the RH^{+H2} and in the $Ni(H_2O)_6$ complex (Figure 1, inset, trace c; Table 1) and the absence of a shoulder in the edge of the RH^{+H2} corroborate this notion.

Effect of Binding of H to the Ni. In standard hydrogenases and in the RH, evidence has been obtained by EPR measurements (*53*, *54*) and by DFT calculations (*16*, *42*−*44*) that in the Ni-C state [e.g., in the RH^{+H2} (*15*, *53*, *54*)] a hydride is present as a bridging ligand between the Ni and Fe atoms. Could the binding of H to the Ni account for the drastic changes in the XANES spectrum of the RH^{+H2}? There are three options for hydride binding: (1) H replaces an S ligand, (2) H replaces an (O,N) ligand, and (3) H binds as an additional ligand to the Ni. Both XAS studies on Ni model compounds and on [NiFe] hydrogenases and XANES simulations contribute relevant information for distinguishing between these possibilities.

The first option leads to agreement with the result obtained in a model study (*29*) that the replacement of a soft S ligand with H (P_4S vs P_4H coordination) strongly increases the maximum of the K-edge [Figure 3 (×)] to a value which is similar to the one obtained via a replacement with O (*29*). If H replaces S, it seems to "mimic" a hard (O,N) ligand. Accordingly, the exchange of (O,N) with H is not expected to cause a significant change in the K-edge maximum, thus rendering the second option unlikely. The question how hydride binding without replacement of any ligand (third option) affects the XANES spectrum is more difficult to answer. In the [NiFe] hydrogenase from *Chromatium vinosum*, in the Ni-S_{i-r} state the Ni seems to be bound by only four S ligands whereas in the Ni-C state a slightly increased K-edge maximum is observed which is compatible with a five-coordinated Ni [Figure 3 (◆)] (*37*). However, the small pre-edge peak in the Ni-C state is suggestive of six-coordinated Ni; the sixth ligand has been attributed to (O,N) (*37*). If the Ni-C state is converted to a Ni-L state, a transition which has been proposed to reflect solely the photolysis of the bound H (*72*), the edge maximum remains approximately unchanged; the pre-edge, however, now suggests a five-coordinated Ni (*37*). At variance with additional H binding, an additional (O,N) ligand [N_3S_2 vs $N_3(O,N)_1S_2$ coordination] in a Ni model (*32*) decreases the pre-edge peak area and, at the same time, pronouncedly increases the K-edge maximum [Figure 3 (∗)]. Assuming the presence of hydride in the Ni-C state, the diverging results about the number of Ni ligands obtained for standard hydrogenases can be reconciled if the binding (or photolysis) of an *additional* H in a given Ni coordination only marginally affects the K-edge maximum but affects the pre-edge peak magnitude. This conclusion renders unlikely the possibility that in the RH the hydride binding takes place without sulfur replacement (third of the above options).

Ab initio simulations of the Ni K-edge on the basis of full multiple-scattering calculations using the FEFF 8.2 code (*66*; see the legend of Figure 4 for details) reproduced the above effects of changing numbers and chemical identity of Ni ligands on the XANES spectra. XANES simulations were carried out on the basis of the crystal structure (1.4 Å resolution) of the reduced state of the *Desulfovibrio vulgaris* [NiFe] hydrogenase where the Ni is coordinated by four thiol ligands (see the inset of Figure 4) (*65*). A simulation of the reported structure yielded a XANES spectrum [Figure 4 (—)] similar to the ones typically observed for standard hydrogenases. A simulation after the insertion of a H atom into the structure in a bridging position between the Ni and Fe atoms (∼1.8 Å away from the Ni) and leaving the other

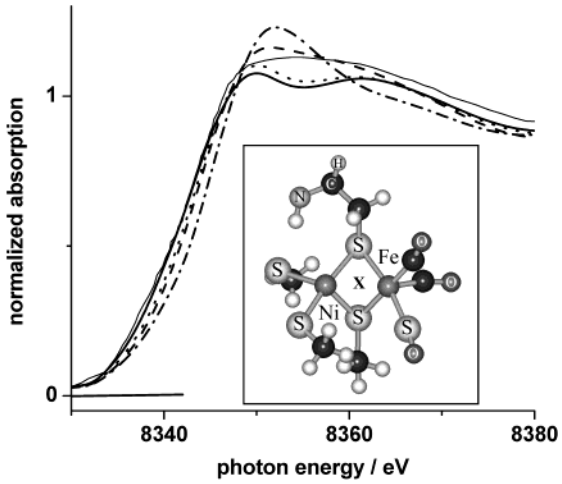

FIGURE 4: Results of *ab initio* simulations of the Ni K-edge. Calculations were carried out using FEFF 8.2 (*66*) with the full multiple-scattering and self-consistent-field options activated and otherwise using default parameters of the program. To obtain coordinates of the atoms of the Ni−Fe site, the crystal structure of the reduced standard [NiFe] hydrogenase of *D. vulgaris* Miyazaki F [structure 1H2R in the Protein Data Bank, 1.4 Å resolution, S_4 Ni coordination (*65*)] was used and supplemented with capping hydrogens (see the inset). The following simulations are shown: 1H2R structure (solid line), 1H2R structure with an H atom in a bridging position (denoted by X) between Ni and Fe (1.8 Å from the Ni) (dotted line), 1H2R structure with an O atom in a position similar to that of the H (1.95 Å from Ni) (dashed line), and similar with an H atom in a bridging position and additionally moving the lower bridging S (see the inset) to 3.8 Å from the Ni (dashed and dotted line). All simulated spectra have been smoothed by adjacent averaging over 7 eV and multiplied by a factor of 0.96 for better comparison between calculated and experimental spectra. No attempts have been made to optimize the simulations by manipulation of simulation parameters. The thin line represents the experimental XANES of the oxidized *D. gigas* hydrogenase (data reproduced from ref *55*) where the Ni is known to be O_1S_4-coordinated (*17*).

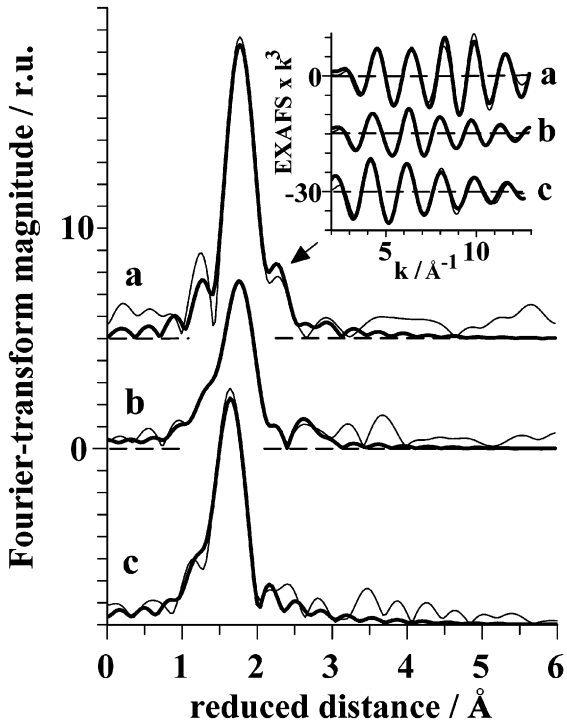

FIGURE 5: Fourier transforms of EXAFS spectra of the RH: (a) RH^{ox} (as-isolated), (b) RH^{+H2} (H_2 flushing for 10 min), and (c) $Ni(H_2O)_6$ from a 5 mM aqueous $NiCl_2$ solution. In traces a−c, experimental data are shown as thin lines and thick lines represent the results of simulations (see Table 2) according to approaches V (RH^{ox}), IX (RH^{+H2}), and X [$Ni(H_2O)_6$], respectively. Spectra have been vertically displaced for better comparison. The inset shows the back-transforms of Fourier transforms into the *k* space using a window of 0.8−3 Å. The arrow marks the shoulder on the main FT peak possibly attributable to a contribution from a Ni−Fe vector (see the text).

atoms in their original positions produced a spectrum with approximately the same magnitude of the edge maximum [Figure 4 (•••)]. Upon the insertion of an oxygen as the fifth ligand (1.95 Å from Ni), however, a significant increase in the K-edge maximum was observed [Figure 4 (− − −)], similar to that in the XANES spectrum of the oxidized form (O_1S_4 Ni coordination) of the *D. gigas* hydrogenase (shown in Figure 4 as a thin line for comparison). An even larger increase in the K-edge maximum was obtained if one of the bridging sulfurs was detached from the Ni in the presence of the bridging H [Figure 4 (−•−)].

In summary, (i) the pronounced change in the edge shape and intensity in the RH^{+H2} cannot be explained simply by the additional binding of a H species leading to a six-coordinated Ni in the Ni-C state. A further structural change is likely. (ii) Assuming the presence of a bound H in the Ni-C state, the following possibilities best explain the changes in the XANES spectrum: one S ligand is detached from the Ni and is replaced with either the H or an (O,N) ligand; in the case of replacement by hydrogen, one further (O,N) ligand binds.

EXAFS Spectra

Figure 5 shows the Fourier transforms of the EXAFS spectra of the RH^{ox} (trace a) and RH^{+H2} (trace b). The inset of Figure 5 shows the Fourier isolates (back-transforms of appropriately "windowed" FTs into the *k* space). Immediately evident is the drastic decrease in the FT magnitude of the RH^{+H2}, suggesting a significant structural change at the Ni in line with the XANES results. Both EXAFS spectra exhibit one major peak around 1.8 Å of a reduced distance (the latter is ∼0.4 Å smaller than the actual absorber−back-scatterer distance). The spectrum of $Ni(H_2O)_6$ (Figure 5, trace c) also shows one major peak, but located at a smaller reduced distance (∼0.2 Å shorter). Thus, from qualitative comparison of spectra, it is immediately obvious that Ni in the RH is likely mixed ligand-coordinated [by (O,N), typical Ni−(O,N) bond lengths of ∼2 Å, and by S, typical Ni−S bond length of ∼2.2−2.4 Å (*55*)]. A smaller magnitude of the EXAFS oscillations of the RH^{+H2} [comparable to the spectrum of the $Ni(H_2O)_6$ complex, inset of Figure 5] at high *k* values is observed. In this *k* region, the oscillations are expected to be dominated by the contributions from higher-*Z* back-scatterers, i.e., sulfur atoms. This observation suggests a decrease in the number of S ligands in the RH^{+H2}.

Simulation of EXAFS Oscillations. EXAFS spectra of the RH^{ox} and RH^{+H2} samples were simulated under variation of the numbers of S and (O,N) ligands, furthermore guided by our results of the XANES analysis. The simulation parameters are listed in Table 2. Simulation curves are shown as thick lines in Figure 5. The EXAFS spectrum of the RH^{ox} was first simulated using only two shells of ligands [(O,N) and S] and assuming a five-coordinated Ni. Oxygen and

Table 2: Simulation Parameters of EXAFS Spectra of the RH[a]

state	fit	shell	coordination no. N_i, per Ni	distance R_i (Å)	σ (Å)	R_F (%) (1.3−2.5 Å)	BVS
RH^{ox}	I	O,N	3	2.07	0.06	18.7	1.99
		S	2	2.18	0.04		
	II	O,N	2	2.06	0.05	15.6	2.25
		S	3	2.17	0.04		
	III	S	4	2.18	0.05	22.7	2.07
	IV	O,N	1	2.06	0.03	20.7	2.48
		S	4	2.17	0.06		
	V	O,N	2	2.06	0.05	16.9	2.27[b]
RH^{+H2}	VIa	O,N	4	2.04	0.12	3.7	2.96
		S	2	2.22	0.06		
	VIb	O,N,(H)	3	2.01	0.11	3.8	nd[c]
		S	2	2.22	0.06		
	VIIa	O,N	3	2.03	0.15	4.0	3.21
		S	3	2.22	0.07		
	VIIb	O,N,(H)	2	1.97	0.14	4.5	nd[c]
		S	3	2.21	0.07		
	VIII	O,N	2	2.05	0.14	9.1	3.44
		S	4	2.20	0.09		
	IX	O,N	4	2.04	0.11	3.0	2.96[b]
		S	2	2.22	0.06		
		Fe	1	3.00	0.12		
RH^{+H2}	VIa	O,N	4	2.04	0.12	3.7	2.96
		S	2	2.22	0.06		
$Ni(H_2O)_6$	X	O	6	2.03	0.07	10.4	2.13

[a] Coordination numbers and R_F values in parentheses refer to the figures which are obtained if the coordination number is not fixed to integer values during the simulation procedure. The filtered *R* factor (*49*), R_F, represents the deviation between data and simulation (in percent) for reduced distances here ranging from 1.3 to 2.5 Å. The $2\sigma^2$ value is the EXAFS Debye−Waller factor. The bond valence sum (BVS, eq 1 in the text) was calculated with a *B* of 0.37 (*50*), using R_{0i} values for Ni(II) of 1.647 Å for Ni−O and 1.937 Å for Ni−S and, for Ni(III), of 1.731 Å for Ni−O and 2.040 Å for Ni−S vectors (data taken from ref *39*). The R_i values are derived from the EXAFS analysis. [b] The Fe atom has not been included in the BVS calculations. [c] Simulations where the BVS has not been calculated (nd) have been carried out under reduction of the number of (O,N) ligands in the corresponding approaches by one to mimic the presence of a Ni-bound H species (see the text).

nitrogen can hardly be distinguished by EXAFS analysis because of their similar back-scattering amplitude. (So far, however, no nitrogen ligation of Ni has been observed in any of the crystal structures; the presence of just oxygen ligands thus seems to be more likely.) Simulations with $(O,N)_3S_2$ and $(O,N)_2S_3$ coordinations (fits I and II, respectively) yield a somewhat better result for the $(O,N)_2S_3$ approach as judged by the smaller R_F (see the footnote of Table 2). The approach with three S ligands seems also to be more compatible with the XANES (see Figure 3). A simulation with exclusively four S ligands yields a clearly larger R_F value and, thus, a less favorable result (fit III). A simulation with $(O,N)_1S_4$ (fit IV) is somewhat worse than the $(O,N)_2S_3$ approach. Furthermore, in this case, the bond valence sum (BVS; see below) is calculated to be 2.45 (Table 2) and thus at the upper limit of the range of 2 ± 25% (*39*) which is compatible with a Ni(II) state.

In several XAS studies on [NiFe] hydrogenases, others have attempted by simulation of EXAFS spectra to discriminate between terminal sulfur ligands and those that bridge the Ni and Fe atoms (*24*, *34*, *37*, *55*). The bond lengths of bridging ligands have been frequently observed to significantly exceed the ones of terminal ligands (see ref *55* and references therein). In the case of the RH^{ox}, even the simulation with four S ligands [$(O,N)_1S_4$ approach] yields a small Debye−Waller parameter of the sulfur shell ($\sigma \sim 0.06$ Å; fit IV in Table 2). This result implies that the bond lengths of the putative terminal and bridging sulfurs deviate by not more than ∼0.1 Å. Such a small deviation precludes a reasonable splitting of the single sulfur shell into two such shells in the simulations. A splitting is furthermore problematic as can be concluded on basis of the Nyquist theorem giving the number of parameters which can be determined independently from simulation of a single EXAFS spectrum (*68* and references therein). Using a Δk of 10.5 $Å^{-1}$ and a ΔR of 1 Å, the maximally allowed number of parameters is calculated to be approximately seven. Thus, the use of three ligation shells would imply that the number of parameters is at the upper limit. It should be noted that, if a simulation is nevertheless carried out with two S shells, the fit quality is not improved (not documented).

In the crystallized standard [NiFe] hydrogenases, the Fe atom has been located within 3 Å of Ni (*2*, *20*, and references therein). Including an Fe atom in the simulation procedure of the EXAFS spectrum of the RH^{ox} yields reasonable results (fit V) but does not improve the quality of the fit. However, this simulation approach more readily accounts for the shoulder on the main FT peak at a reduced distance of ∼2.3 Å (Figure 3, trace a, arrow). [A shoulder on the main FT peak was also observed (not shown) in the incompletely oxidized as-isolated sample (see Figure 1), indicating that this feature is not due to noise contributions.] The putative Fe coordination shell shows a relatively large Debye−Waller parameter (Table 2) pointing to a large statical disorder in this shell (large distance spread) or to contributions from secondary back-scatterer shells (*24*). If an Fe atom can be discerned in the EXAFS spectrum, its distance from Ni should be 2.73 Å in the RH^{ox}.

The XANES spectrum of the RH^{+H2} implies a six-coordinated Ni site, with an increased number of non-sulfur ligands. The first problem in the EXAFS simulations is the chemical nature of the sixth ligand. One possibility is that it is a hydride (*53*, *54*) (see the XANES section). Such a bound H is not expected to be visible in the EXAFS spectrum due to the fact that its back-scattering amplitude is almost negligible compared to those of (O,N) or S ligands (*29*, *64*). We simulated the RH^{+H2} spectrum by assuming a six-coordinated Ni site with only (O,N) and S ligands and, alternatively, by reducing the number of (O,N) ligands by one (to mimic the presence of a bound H which was not explicitly included in the fits). The assumption of an $(O,N)_4S_2$ or $(O,N)_3(H_1)S_2$ coordination of the Ni yields very good fit results (very low R_F values) (Table 2, fits VIa and VIb). A simulation with $(O,N)_3S_3$ or $(O,N)_2H_1S_3$ produces a comparable fit quality (Table 2, fits VIIa and VIIb). An $(O,N)_4S_2$ or $(O,N)_3H_1S_2$ coordination, however, may be more compatible with the XANES spectrum of the RH^{+H2} (compare Figure 4). Using four S ligands [$(O,N)_2S_4$] yields a result which is not in good agreement with the EXAFS data (the R_F value is approximately doubled; fit VIII). Inspection of the fit results from the above approaches reveals that the Debye−Waller parameters (σ) of the S shell are relatively low. Splitting the S shell into two such shells consequently results in Ni−S distances which differ by not more than ∼0.1 Å; however, this does not improve the fit results (not shown). On the other hand, the Debye−Waller parameter of the (O,N) shell is large when, for instance, compared to the result of the simulation of the EXAFS spectrum of the $Ni(H_2O)_6$

complex (Table 2, fit X). This result implies the presence of ligands with significantly different Ni−(O,N) bond lengths in the RH^{+H2}. This finding may support the idea that one (O,N) ligand is in fact a H ligand. As already observed in the case of the RH^{ox}, the inclusion of a further Fe atom does not yield improved fit results (fit IX represents an example of such an approach). If Fe is detectable, in the RH^{+H2} its distance from the Ni would be larger than in the RH^{ox} (namely, 3 Å). Simulations according to approach IX, including an Fe atom of several spectra from incompletely oxidized as-isolated and short-time hydrogen-incubated RH samples (see Figure 1) with various mixtures of the RH^{ox} and RH^{+H2} states, yielded Ni−Fe distances between 2.74 and 2.91 Å (not documented). These values which are larger than the one derived for the pure RH^{ox} (2.73 Å) further corroborate an increased Ni−Fe distance in the RH^{+H2}. It is worth noting that an increase in the Ni−Fe distance has also been observed in other hydrogenases upon oxidation of the Ni (*34*−*37*).

In the RH^{+H2}, a lengthening of the Ni−S vectors is also observed (Table 2). Upon formation of Ni(III), a shortening of Ni−S distances is expected (*38*), whereas an overall lengthening is expected if the Ni coordination changes from five to six (*55*). Thus, the observed distance increase may be taken as further evidence for the presence of six-coordinated Ni in the RH^{+H2}. For both the RH^{ox} and the RH^{+H2}, the average Ni−S bond lengths determined here are at the lower limit of what has been reported both for five- and six-coordinated Ni model compounds and also for the Ni−S bond lengths of bridging S ligands (*55*). However, there is clearly no indication for Ni−S vectors to the RH EXAFS of significantly more than ∼2.2 Å. Any inclusion of longer Ni−S distances, namely, of 2.3−2.6 Å (which have been reported for bridging S ligands), in the simulations (with or without the further inclusion of a Ni−Fe vector) yields unsatisfying results showing unreasonably high R_F values and/or irrationally large or physically meaningless negative Debye−Waller parameters of the S shells (not documented). As noted previously (*37*, *55*), to render the EXAFS oscillations of long Ni−S vectors almost invisible, they have to be comparable in length to the Ni−Fe vector. Such a situation will give rise to destructive interference between both oscillations due to their almost counter-phasic behavior. To obtain such a situation, in the case of the RH, the Ni−S distance has to be >2.6 Å, and thus unreasonably long for an S ligand in the first coordination sphere. Because of these principal limitations of the EXAFS analysis, we cannot completely rule out the presence of sulfur at greater distances from the Ni in the RH; however, we consider it to be less likely.

Comparison of k^1- and k^3-Weighted Spectra. Due to the fact that in EXAFS simulations the coordination number (N_i) and Debye−Waller parameter ($2\sigma_i^2$) are highly correlated for a given first-sphere back-scatterer shell, the uncertainty in the coordination number is on the order of ±1 in the simulations presented in Table 2. Here, this uncertainty is specifically relevant with regard to the number of S ligands that coordinate the Ni which, in standard hydrogenases, largely determine the overall structure of the Ni site. It has been shown that unique N_i and $2\sigma_i^2$ couples can be obtained if a simulation of k^1- and k^3-weighted EXAFS oscillations is performed under minimization of a common error factor (*67*, *68*). In Figure 6, the results of such a simulation on the

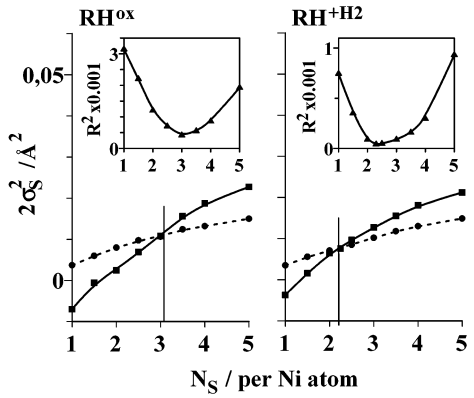

FIGURE 6: Plot of the Debye−Waller parameter vs the coordination number of the S shell. Points are the result of simulations of k^1-weighted (■) and k^3-weighted (●) EXAFS oscillations using one (O,N) and one S shell of back-scatterers in the first Ni coordination sphere with variation of the number of S ligands. The common error factors (here defined as $R^2 = R_{F,k1}^2 + R_{F,k3}^2$) are shown in the insets. Points are connected by smooth lines to guide the eye: (left) RH^{ox} and (right) RH^{+H2}. Vertical lines mark the positions of the crossing points on the N_S scale.

RH^{ox} and RH^{+H2} spectra under variation of N_S (the coordination number of the S shell) are shown. In both cases, a plot of $2\sigma_S^2$ versus N_S results in approximately straight lines for k^1- and k^3-weighted spectra, however, with different slopes. The crossover point of these lines (equal to $2\sigma^2$, vertical lines in Figure 6) is found at $N_S \sim 3.1$ in the case of the RH^{ox} and at a lower N_S value (∼2.2) in the case of the RH^{+H2}. Only using these N_S and $2\sigma_S^2$ pairs, the common error factor becomes minimal (insets of Figure 6). These results are compatible with the notion that the number of S ligands in the RH^{ox} ($N_S = 3$) decreases in the RH^{+H2} to a value of 2.

Bond Valence Sum Calculations. The method of bond valence sum calculation (BVS) has been successfully used to test the validity of oxidation state assignments and metal coordination number determinations in metalloenzymes (*39*). If a structural model is deduced from XAS data, the BVS can be used to confirm the compatibility of the model with a given oxidation state. The BVS is calculated (for values of R_{0i} and B, see the footnote of Table 2) according to (*39*)

$$\mathrm{BVS} = \sum_{i=1}^{n} \exp[(R_{0i} - R_i)/B] \qquad (1)$$

With the possible exception of fit IV (four S ligands), the BVS values are close to 2 for all fit approaches used for the RH^{ox} EXAFS (Table 2) and, thus, compatible with the assumed Ni(II) oxidation state in the RH^{ox}. Assuming a Ni(III) yielded BVS values clearly deviating from 3 (not shown). Again, with the possible exception of fit VIII (four S ligands), all BVS values that were calculated for the RH^{+H2} are close to 3, in agreement with the assumption of a Ni(III) state (Table 2). Apparently, the BVS calculations seem to be again more compatible with a coordination of the Ni by less than four S ligands in both forms of the RH. Taking the results of the analysis of XANES and EXAFS spectra and of the BVS calculations together, we feel that the corresponding EXAFS simulation approaches where the number of S ligands decreases by one in the RH^{+H2} (e.g., from 3 to 2) are more likely.

DISCUSSION

Comparison of the Ni Sites in the Oxygen-Insensitive and Standard [NiFe] Hydrogenases. The analysis of Ni XAS spectra of the hydrogen sensor, RH, in this work unravels a feature, namely, a pronounced structural change at the Ni site upon formation of the Ni-C state of the enzyme, that is seemingly unprecedented in any of the oxygen-sensitive [NiFe] hydrogenases studied so far. A marked, but not identical, structural change has only been detected in one other oxygen-resistant hydrogenase, the SH of *R. eutropha* (*24*, *34*). Crystallography (*3*, *20*, and references therein) and XAS studies (*24*, *37*, *40*, *55*) on several standard hydrogenases have consistently revealed that the Ni binding is facilitated by four thiol ligands which originate from conserved cysteine residues that are present in all sequences of the large subunits of [NiFe] hydrogenases known so far (for a review, see ref *6*). X-ray analysis as well as XAS studies revealed that the nickel binding by the four cysteine residues is independent of the oxidation state of these enzymes; e.g., in the *C. vinosum* hydrogenase, the Ni is coordinated by the four cysteine ligands in all seven oxidation states of the protein (*37*). In the hydrogenase from *T. roseopersicina*, there is indication for a Ni that may be bound by only two cysteine ligands (*24*, *41*), this feature, however, being again independent of oxidation state (*63*).

At first glance, several findings may imply a binding of the Ni in the oxygen-insensitive hydrogenases of *R. eutropha* similar to the one observed in standard hydrogenases. In case of the RH, the amino acid sequence of the large subunit HoxC also contains four conserved cysteine residues which have been designated as putative nickel-binding ligands (*11*). In case of the SH, studies with site-directed mutant proteins revealed that three of the four conserved cysteine residues of the large subunit HoxH are required for proper nickel insertion and that all four residues are essential for the formation of a catalytically active SH protein (*62*). However, XAS studies on the RH (this work) and on the SH (refs *24* and *34* and unpublished observations of T. Burgdorf and M. Haumann) clearly imply a different situation in the oxygen-insensitive [NiFe] hydrogenases, namely, (1) the coordination of Ni by fewer than four thiol ligands and (2) a change in the number of S ligands upon formation of the Ni-C state. We have found in this work that in the oxidized state of the RH the Ni(II) is likely bound by only three sulfur ligands that presumably originate from cysteine residues. In the hydrogen-treated state of the RH (Ni-C state), the number of S ligands that bind the Ni(III) is likely reduced by one as detected by XAS. In the SH, the opposite has been observed. The presence of only two or even fewer S ligands to the Ni(II) has been detected in the oxidized SH (*24*, *34*; see also Figure 3). If a Ni-C EPR signal [Ni(III)] can be observed for the SH after harsh chemical reduction (*14*), however, the number of S ligands to the Ni has been reported to be increased to 3 or 4 (*24*, *34*). [Whether the reported Ni-C state of the SH is physiologically relevant or whether it is a result of the harsh reductive treatment of the enzyme is under debate (*12*) and will be investigated in a forthcoming publication (Burgdorf et al., 2003, manuscript in preparation).] Thus, it seems as if only a specific subset of the four putative cysteine ligands found in the amino acid sequences of both the RH and the SH are actually employed in the binding of Ni, furthermore depending on the oxidation state. It is tempting to speculate that the specific Ni coordination and its dynamics in the catalytic cycle are crucial for the specific functions and for the oxygen insensitivity of the hydrogenases of *R. eutropha*. Further studies using site-directed mutagenesis of the RH are underway and expected to allow for the discrimination of the Ni-binding cysteines.

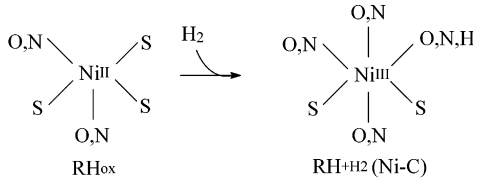

FIGURE 7: Coordination of the Ni in the RH^{ox} and RH^{+H2} (Ni-C state) derived from XAS data analysis.

Interestingly, in the Ni-C state, the Ni(III) has been found to be coordinated by different numbers of thiol ligands, namely, by four [*D. gigas* (*17*), *D. vulgaris* (*65*), and *C. vinosum* (*37*)], four or three [*Desulfovibrio baculatus* (*36*) and SH of *R. eutropha* (*24*, *34*)], or two [*T. roseopersicina* (*63*) and RH of *R. eutropha* (this work)]. In all of the latter enzymes, a "normal" Ni-C EPR signal with discernible but only minor variations in *g* values has been observed (*14*, *15*, *63*, *69*−*72*). The latter is true (*69*) even for the NiFeSe hydrogenase of *D. baculatus* where the Ni is coordinated by three thiol groups and one Se from a selenocysteine (*36*). Seemingly, the presence of similar EPR signals characteristic for the Ni(III)-C state does not necessarily indicate that the Ni ligand environment is identical.

Apparently, several different Ni coordinations in [NiFe] hydrogenases are compatible with the same function, hydrogen cleavage. A similar observation has been made in other metalloenzymes where catalytic activity is in part retained if ligands to the metal are exchanged by site-directed mutagenesis (for an example, see ref *59*). The unusual combination of Ni coordinations and oxidation states in the RH (see below) and the SH (*12*, *14*) suggests that also mechanistically these enzymes differ from the standard hydrogenases (*16*, *42*−*44*). The specific coordination of the Ni in the RH may "tune" the Ni site with respect to a particular physiological function, i.e., hydrogen sensing versus hydrogen cleavage.

Structural Changes at the Ni and a Tentative Scheme for Hydrogen Sensing by the RH. The data that have been derived directly from our XAS analysis are summarized in a model of the structure of the Ni site of the RH as illustrated in Figure 7. In the absence of hydrogen, the Ni(II) in the RH^{ox} is five-coordinated, implying one vacant binding site. By analogy with the standard hydrogenases, we anticipate that the RH^{ox} is in a formal "ready" state, termed Ni-S in the context of the standard hydrogenases (*24*, *37*, *41*), accounting for the capacity of the RH to immediately react with hydrogen without the necessity for reductive activation (*15*). Upon the addition of hydrogen, a pronounced structural change occurs. Then, a saturated six-coordinated Ni(III) is formed. The absence of O_2 and CO binding to Ni in the Ni-C state of the RH (*15*) is compatible with this notion. The Ni coordination environments shown in Figure 7, however, pronouncedly differ from the respective ones of standard hydrogenases. In both states, the number of S ligands to the Ni is fewer than four. Moreover, a decrease in the number

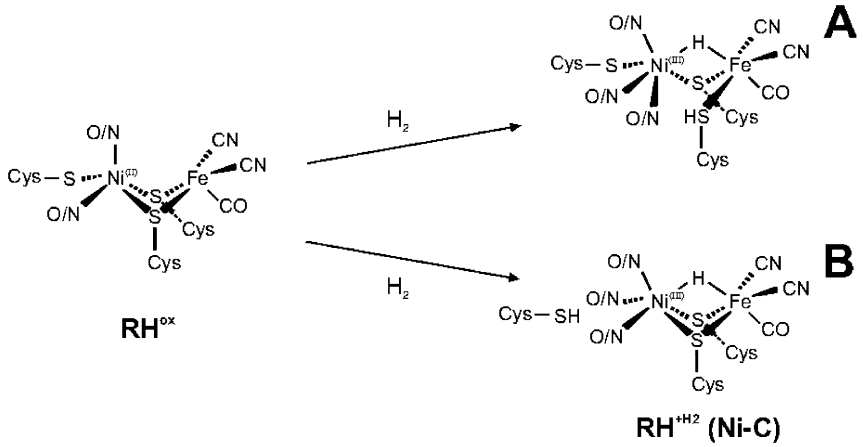

FIGURE 8: Two alternative schemes for structural changes at the [NiFe] site in the hydrogen sensor RH.

of S ligands by one is postulated upon formation of the Ni-C state.

It is tempting to speculate about a more detailed model of the reactions of the RH during hydrogen sensing on the basis of the XAS results of this study and on the basis of the biochemical and spectroscopic data outlined in refs *11*, *13*, and *15*. In previous studies, it was shown by FTIR analysis that the [NiFe] active site of the RH contains one CO and two CN ligands attached to the Fe (*13*, *15*). EPR studies revealed that the Ni and not the Fe is redox active. The EPR spectra of the Ni-C state of the RH were very similar to those obtained for the standard hydrogenases (*13*, *15*). Since the amino acid sequence of the RH large subunit, HoxC, also contains the four conserved cysteine residues (see above), it was proposed in the previous studies that the structure of the RH [NiFe] active site is very similar or even identical to those of the standard hydrogenases. A detailed ENDOR study showed for the first time experimentally the binding of a hydrogen ligand in the bridging position between the Ni and the Fe in the Ni-C state of the RH (*53*, *54*). Upon illumination at low temperatures, the Ni-C state is converted to Ni-L in standard hydrogenases; the latter state has been proposed to result from the photolysis of the bridging hydride, yielding a formal Ni(I) oxidation state (*72*). This theory has gained strength from the analysis of ENDOR data of the RH (*53*, *54*); the light sensitivity that has also been observed in the RH (*13*, *15*) was due to the photolysis of the bridging H ligand. The Ni-L EPR signal reveals somewhat altered *g* values with respect to the standard hydrogenases; the photolyzed H was found to be in the vicinity (~4 Å) of Ni (*53*, *54*).

The information from these data in combination with the XAS results of this study is summarized in Figure 8, showing structural models for the RH active site which have been constructed in analogy to the structure of the active site in standard hydrogenases, assuming the presence of two sulfur bridges between Ni and Fe in the RH^{ox}. (1) Upon exposure of the RH to hydrogen, in the Ni-C state a hydride is inserted as a bridge between the Ni and Fe atoms. (2) Two possibilities for the detachment of a sulfur from the Ni in the Ni-C state are advisable. They are depicted in structures A and B of Figure 8. At variance with the situation in standard hydrogenases, concomitantly with the hydride binding the protonation of one bridging sulfur may occur. The protonation leads to the loss of the coordination between the sulfur and the Ni as suggested by DFT calculations (*42*), causing a decrease in the number of S ligands to the Ni of one (Figure 8A). Alternatively, concomitantly with the hydride binding, a terminal sulfur may be detached from the Ni and replaced with an (O,N) ligand (Figure 8B). (3) One specific feature of the RH is the absence of the binding of O_2 and CO to the Ni-C state (*15*). These molecules might be excluded from the active site by their limited accessibility from the bulk. A more likely option for preventing their binding is an (O,N) ligand from an amino acid or from an intrinsic water molecule that occupies the sixth ligand position at the Ni. A further possibility, although elegant, namely, the formation of a CN bridge between Ni and Fe from a CN ligand of the Fe as proposed from DFT calculations (*42*), may be less likely on the basis of FTIR results (*15*). (4) In the RH, the electron that is derived from the oxidation of the Ni is possibly directed not to an Fe−S cluster but to the putative nonmetal redox cofactor (*15*). It has been shown in studies with Ni model compounds that the mixed ligation of Ni by S and, for example, heterocyclic N ligands increases the midpoint potential of the Ni(III)/Ni(II) pair compared to predominant coordination of Ni by electron-rich (thiolate) ligands (*32*, *47*). Thus, the midpoint potential of the Ni(III)/Ni(II) pair may be too positive to reduce Fe−S clusters in the presence of a more (O,N)-rich ligation of the Ni, compatible with the absence of Fe−S cluster reduction in the RH^{+H2} (*13*, *15*). (5) The Ni(III) state, while being a formal "active" (Ni-C) state, is nevertheless a "blind alley" (in terms of hydrogen turnover) where the RH becomes temporarily stuck, leading to the unusual stability of the Ni-C state in the RH (*13*, *15*). A sulfur-rich Ni coordination has been postulated to be a prerequisite for the formation of a transient Ni(I) state involved in hydrogen cleavage subsequent to the formation of the active Ni(III) (Ni-C) state in standard hydrogenases (*32*, *43*, *48*). The more (O,N)-rich Ni coordination in combination with the loss of one sulfur bridge may thus trap the [NiFe] site in a configuration which mimics certain features of the transition state structure [the presence of a Ni(III)−H bond, for example] but which lacks the key elements that promote normal reactivity, thereby blocking the formation of subsequent reaction intermediates in the RH. The nature of these key elements still needs to be elucidated. (6) The electron that is released from the [NiFe] active site upon binding of H_2 is transferred to the nonmetal redox cofactor. In the RH^{+H2}

state, the RH activates the HoxJ−HoxA two-component system that controls the expression of the energy-converting hydrogenases. The signal is switched off when the electron flows back from the nonmetal cofactor to the [NiFe] active site, finally releasing an H_2 molecule and reconverting the RH into its RH^{ox} state. Thus, the RH is a very efficient "all-or-none" hydrogen detector that triggers hydrogenase gene expression in *R. eutropha*.

CONCLUSIONS

X-ray absorption spectroscopy at the Ni K-edge on the oxygen-insensitive regulatory [NiFe] hydrogenase (RH) from *R. eutropha* reveals that a pronounced structural change at the Ni is induced in the presence of hydrogen. The XAS data are best explained under the assumption that the aerobically isolated Ni(II) state (RH^{ox}) with $(O,N)_2S_3$ coordination is converted to a Ni(III) (Ni-C) state (RH^{+H2}) with $(O,N)_3X_1S_2$ coordination [X may be an (O,N) or H ligand]. There is evidence for a bound H in the Ni-C state; the origin of the new (O,N) ligand is an open question. Further studies on site-directed mutants may help in elucidating the role of specific amino acid residues in the structure and function of the RH Ni site. The XAS data from the RH provide first clues that its function, hydrogen sensing, may be largely determined by the unusual Ni ligand environment and its "dynamic" behavior.

ACKNOWLEDGMENT

We are indebted to the staff at the EMBL Outstation in Hamburg for excellent technical assistance. We thank Profs. S. Albracht and G. Henkel and Dr. M. Brecht for stimulating discussions and Dr. F. Lendzian, M. Kammel, and M. Galander for generous support with respect to the EPR experiments.

REFERENCES

1. Albracht, S. P. (1994) *Biochim. Biophys. Acta 1188*, 167−204.
2. Happe, R. P., Roseboom, W., Pierik, A. J., Albracht, S. P., Bagley, K. A., Happe, T., Mosler, B., and Naber, J. (1997) *Nature 385*, 126.
3. Cammack, R., Robson, R., and Frey, M., Eds. (2001) *Hydrogen as a fuel: Learning from nature*, Taylor & Francis, London.
4. Maroney, M. J., and Bryngelson, P. A. (2001) *J. Biol. Inorg. Chem. 6*, 453−459.
5. Frey, M. (2002) *ChemBioChem 3*, 153−160.
6. Vignais, P. M., Billoud, B., and Meyer, J. (2001) *FEMS Microbiol. Rev. 25*, 455−501.
7. Lenz, O., and Friedrich, B. (2001) *Biospectrum 6*, 515−520.
8. Lenz, O., Bernhard, M., Buhrke, T., Schwartz, E., and Friedrich, B. (2002) *J. Mol. Microbiol. Biotechnol. 4*, 255−262.
9. Schneider, K., and Schlegel, H. G. (1976) *Biochim. Biophys. Acta 8*, 66−88.
10. Lenz, O., and Friedrich, B. (1998) *Proc. Natl. Acad. Sci. U.S.A. 95*, 12474−12479.
11. Kleihues, L., Lenz, O., Bernhard, M., Buhrke, T., and Friedrich, B. (2000) *J. Bacteriol. 182*, 2716−2724.
12. Happe, R. P., Roseboom, W., Egert, G., Friedrich, C. G., Massanz, C., Friedrich, B., and Albracht, S. P. (2000) *FEBS Lett. 466*, 259−263.
13. Pierik, A. J., Schmelz, M., Lenz, O., Friedrich, B., and Albracht, S. P. (1998) *FEBS Lett. 438*, 231−235.
14. Schneider, K., Erkens, A., and Müller, A. (1996) *Naturwissenschaften 83*, 78−81.
15. Bernhard, M., Buhrke, T., Bleijlevens, B., De Lacey, A. L., Fernandez, V. M., Albracht, S. P., and Friedrich, B. (2001) *J. Biol. Chem. 276*, 15592−15597.
16. Stein, M., and Lubitz, W. (2002) *Curr. Opin. Chem. Biol. 6*, 243−249.
17. Volbeda, A., Fontecilla-Camps, J. C., and Frey, M. (1996) *Curr. Opin. Struct. Biol. 6*, 804−812.
18. Pierik, A. J., Roseboom, W., Happe, R. P., Bagley, K. A., and Albracht, S. P. (1999) *J. Biol. Chem. 274*, 3331−3337.
19. Schneider, K., and Schlegel, H. G. (1978) *Biochem. Biophys. Res. Commun. 84*, 564−571.
20. Frey, M. (1999) in *Metal Sites in Proteins and Models: Redox Centres* (Hill, H. A. O., Sadler, P. J., and Thomson, A. J., Eds.) pp 97−126, Springer-Verlag, Heidelberg, Germany.
21. Bradford, M. (1996) *Anal. Biochem. 72*, 248−254.
22. Schiller, H., Dittmer, J., Iuzzolino, L., Dörner, W., Meyer-Klaucke, W., Sole, A., Nolting, N.-F., and Dau, H. (1998) *Biochemistry 37*, 7340−7350.
23. Pettifer, R. F., and Hermes, C. (1985) *J. Appl. Crystallogr. 18*, 404−412.
24. Gu, Z., Dong, J., Allan, C. B., Chudhury, S., Franco, R., Moura, J., Moura, I., LeGall, J., Przybyla, A., Roseboom, W., Albracht, S. P., Axley, M., Scott, R., and Maroney, M. J. (1996) *J. Am. Chem. Soc. 118*, 11155−11165.
25. Dittmer, J. (1999) Ph.D. Thesis, Phillips-Universität Marburg, Marburg, Germany.
26. Yachandra, V. K. (1995) *Methods Enzymol. 246*, 638−675.
27. Scott, R. A. (2000) in *Physical Methods in Bioinorganic Chemistry*, pp 465−503, University Science Books, Sausalito, CA.
28. Eidsness, M. K., Scott, R. A., Prickril, B. C., DerVartanian, D. V., LeGall, J., Moura, I., Moura, J., and Peck, H. D. (1998) *Proc. Natl. Acad. Sci. U.S.A. 86*, 147.
29. Colpas, G. J., Maroney, M. J., Bagyinka, C., Kumar, M., Willis, W. S., Suib, S. L., Baidya, N., and Mascharak, P. K. (1991) *Inorg. Chem. 30*, 920−928.
30. Mansour, A. N., and Melendres, C. A. (1998) *J. Phys. Chem. A 102*, 65−81.
31. Roberts, L. M., and Lindahl, P. A. (1995) *J. Am. Chem. Soc. 117*, 2565−2572.
32. Baidya, N., Olmstead, M. M., and Mascharak, P. K. (1992) *J. Am. Chem. Soc. 114*, 9666−9668.
33. Furenlid, L. R., Renner, M. W., and Fujita, E. (1995) *Physica B 208*, 739−742.
34. Müller, A., Erkens, A., Schneider, K., Müller, A., Nolting, H.-F., Sole, V. A., and Henkel, G. (1997) *Angew. Chem. 109*, 1812−1815.
35. Higuchi, Y., Ogata, H., Miki, K., Yasuoka, N., and Yagi, T. (1999) *Struct. Folding Des. 7*, 549−556.
36. Garcin, E., Vernede, X., Hatchikian, E. C., Volbeda, A., Frey, M., and Fontecilla-Camps, J. C. (1999) *Struct. Folding Des. 7*, 557−566.
37. Davidson, G., Choudhury, S., Gu, Z., Bose, K., Roseboom, W., Albracht, S. P., and Maroney, M. (2000) *Biochemistry 39*, 7468−7474.
38. Köckerling, M., and Henkel, G. (1993) *Chem. Ber. 126*, 951−953.
39. Liu, W., and Thorp, H. H. (1993) *Inorg. Chem. 32*, 4102−4105.
40. Scott, R. A., Wallin, S. A., Czechowski, M., DerVartanian, D. V., LeGall, J., Peck, H. D., and Moura, I. (1984) *J. Am. Chem. Soc. 106*, 6864−6865.
41. Maroney, M. J., Colpas, G. J., Bagyinka, C., Baidya, N., and Mascharak, P. K. (1991) *J. Am. Chem. Soc. 113*, 3962−3972.
42. Pavlov, M., Siegbahn, P. E. M., Blomberg, M. R. A., and Crabtree, R. H. (1998) *J. Am. Chem. Soc. 120*, 548−555.
43. Niu, S., Thomson, L. M., and Hall, M. B. (1999) *J. Am. Chem. Soc. 121*, 4000−4007.
44. Amara, P., Volbeda, A., Fontecilla-Camps, J. C., and Field, M. J. (1999) *J. Am. Chem. Soc. 121*, 4468−4477.
45. Trofanchuk, O., Stein, M., Gessner, C., Lendzian, F., Higuchi, Y., and Lubitz, W. (2000) *J. Biol. Inorg. Chem. 5*, 36−44.
46. Müller, A., Tscherny, I., Kappl, R., Hatchikian, E. C., Hüttermann, J., and Cammack, R. (2002) *J. Biol. Inorg. Chem. 7*, 177−194.
47. Krüger, H.-J., and Holm, R. H. (1990) *J. Am. Chem. Soc. 112*, 2955−2963.
48. James, T. L., Cai, L., Muetterties, M. C., and Holm, R. H. (1996) *Inorg. Chem. 35*, 4148−4161.
49. Meinke, C., Sole, A., Pospisil, P., and Dau, H. (2000) *Biochemistry 39*, 7033−7040.
50. Brown, I. D., and Altermatt, D. (1985) *Acta Crystallogr. B41*, 244−247.
51. Zhabinsky, S. I., Rehr, J. J., Ankudinov, A., Albers, R. C., and Eller, M. J. (1995) *Phys. Rev. B 52*, 2995−3009.

52. Musgrave, K., Laplaza, C., Holm, R., Hedman, B., and Hodgson, K. (2002) *J. Am. Chem. Soc. 124*, 3083−3092.
53. Lubitz, W., Brecht, M., Foerster, S., Stein, M., Higuchi, Y., Buhrke, T., and Friedrich, B. (2002) in *EPR in the 21st century* (Kawamori, A., Yamauchi, J., and Ohta, H., Eds.) pp 437−445, Elsevier, Amsterdam.
54. Brecht, M. (2001) Ph.D. Thesis, Technische Universität Berlin, Berlin, Germany.
55. Gu, W., Jacquamte, D. S., Wang, H.-X., Evans, D. J., Smith, M. C., Millar, M., Koch, S., Eichhorn, D. M., Latimer, M., and Cramer, S. P. (2003) *J. Inorg. Biochem. 93*, 41−51.
56. Eidsness, M. K., Sullivan, R. J., and Scott, R. J. (1988) in *The bioinorganic chemistry of nickel. Electronic and molecular structure of biological nickel as studied by X-ray absorption spectroscopy* (Lancaster, J. R., Ed.) pp 73−91, VCH Publishers, New York.
57. Vaarkamp, M., Dring, I. I., Oldman, R. J., Stern, E. A., and Koningsberger, D. C., (1994) *Phys. Rev. B 50*, 7872−7883.
58. Buhrke, T., Brecht, M., Lubitz, W., and Friedrich, B. (2002) *J. Biol. Inorg. Chem. 7*, 897−908.
59. Krüer, M., Haumann, M., Meyer-Klaucke, W., Thauer, R., and Dau, H. (2002) *Eur. J. Biochem. 269*, 1−7.
60. Elsen, S., Colbeau, A., Chabert, J., and Vignais, P. M. (1996) *J. Bacteriol. 178*, 5174−5181.
61. Black, L. K., Fu, C., and Maier, R. J. (1994) *J. Bacteriol. 176*, 7102−7106.
62. Massanz, C., and Friedrich, B. (1999) *Biochemistry 38*, 14330−14337.
63. Bagyinka, C., Whitehead, J. P., and Maroney, M. J. (1993) *J. Am. Chem. Soc. 115*, 3576−3585.
64. D'Angelo, P., Barone, V., Chillemi, G., Sanna, N., Meyer-Klaucke, W., and Pavel, N. V. (2002) *J. Am. Chem. Soc. 124*, 1958−1967.
65. Higuchi, Y., Ogata, H., Miki, K., Yasuoka, N., and Yagi, T. (1999) *Structure 7*, 549−556.
66. Ankudinov, A. L., Ravel, B., Rehr, J. J., and Conradson, R. D. (1998) *Phys. Rev. B 12*, 7565−7576.
67. Koningsberger, D. C. (1994) in *Neutron and Synchrotron Radiation for Condensed Matter Studies* (Baruchel, J., Hodeau, J. L., Lehmann, M. S., Regnard, J. R., and Schlenker, C., Eds.) Vol. II, p 213, Springer, Berlin.
68. Koningsberger, D. C., Mojet, B. L., vanDorssen, G. E., and Ramaker, D. E. (2000) *Top. Catal. 10*, 143−155.
69. He, S. H., Teixeira, M., LeGall, J., Patil, D. S., Moura, I., Moura, J. J., DerVartanian, D. V., Huynh, B. H., and Peck, H. D. (1989) *J. Biol. Chem. 264*, 2678−2682.
70. Barondeau, D. P., Roberts, L. M., and Lindahl, P. A. (1994) *J. Am. Chem. Soc. 116*, 3442−3448.
71. Happe, R. P., Roseboom, W., and Albracht, S. P. J. (1999) *Eur. J. Biochem. 259*, 602−608.
72. Foerster, S., Stein, M., Brecht, M., Ogata, H., Higuchi, Y., and Lubitz, W. (2003) *J. Am. Chem. Soc. 125*, 83−93.
73. Cramer, S. P., Eidsness, M. K., Pan, W., Morton, T. A., Ragsdale, S. W., DerVartanian, D. V., Ljungdahl, L. G., and Scott, R. A. (1987) *Inorg. Chem. 26*, 2477−2479.
74. Dau, H., Liebisch, P., and Haumann, M. (2003) *Anal. Bioanal. Chem. 376* (5), 562−583.

BI034804D